Apparent Changes in Pacific Decadal Variability Caused by Anthropogenically-Induced Mean State Modulations

Chen Xing[1], Samantha Stevenson[1], Emanuele Di Lorenzo[2], Matthew Newman[3], Antonietta Capotondi[4], John T. Fasullo[5], and Nicola Maher[6]

[1]University of California, Santa Barbara
[2]Brown University
[3]NOAA/PSL
[4]University of Colorado/CIRES and NOAA/PSL
[5]National Center for Atmospheric Research (UCAR)
[6]Australian National University, Canberra

November 14, 2024

Abstract

Pacific decadal variability (PDV), low-frequency changes in Pacific sea surface temperatures (SSTs), significantly impacts global climate. However, disentangling anthropogenic effects upon PDV is challenging since both vary on similar time scales. Using single-forcing climate model large ensembles, we find that anthropogenic forcing primarily drives a spatially-varying pattern of mean-state change in North Pacific SST that project onto leading PDV patterns, principally the Pacific Decadal Oscillation (PDO) and North Pacific Gyre Oscillation (NPGO). In fact, when the trend is determined by the model ensemble mean, there is no forced change of the PDV modes. However, analysis of single model realizations, where the mean-state trend cannot be cleanly identified, suggests an apparent anthropogenic change in NPGO decadal variability. This suggests that observed PDV responses to anthropogenic forcing may be erroneously convolved with the background trend pattern. Therefore, correctly determining the mean-state trend is a necessary precursor for identifying forced changes to PDV.

Apparent Changes in Pacific Decadal Variability Caused by Anthropogenically-Induced Mean State Modulations

Chen Xing[1], Samantha Stevenson[1], Emanuele Di Lorenzo[2], Matthew Newman[3], Antonietta Capotondi[3, 4], John Fasullo[5], Nicola Maher[6]

[1] Bren School of Environmental Science & Management, University of California at Santa Barbara, Santa Barbara, CA, USA.

[2] Department of Earth, Environmental & Planetary Sciences, Brown University, Providence, RI, USA.

[3] Physical Sciences Laboratory, NOAA, Boulder, CO, USA.

[4] CIRES, University of Colorado at Boulder, Boulder, CO, USA.

[5] National Center for Atmospheric Research, Boulder, CO, USA.

[6] Research School of Earth Sciences, Australian National University, Canberra, Australian Capital Territory, Australia.

Corresponding author: Chen XIng (chenxing@ucsb.edu)

Key Points:

- In large climate model ensembles, the Pacific Decadal Oscillation does not exhibit a clear response to anthropogenic forcing.
- Anthropogenic forcing does affect the North Pacific, but primarily through the time-varying mean-state trend.
- Forced mean-state trends resemble PDV, making variability changes seem apparent if the background trend isn't correctly removed.

Abstract

Pacific decadal variability (PDV), low-frequency changes in Pacific sea surface temperatures (SSTs), significantly impacts global climate. However, disentangling anthropogenic effects upon PDV is challenging since both vary on similar time scales. Using single-forcing climate model large ensembles, we find that anthropogenic forcing primarily drives a spatially-varying pattern of mean-state change in North Pacific SST that project onto leading PDV patterns, principally the Pacific Decadal Oscillation (PDO) and North Pacific Gyre Oscillation (NPGO). In fact, when the trend is determined by the model ensemble mean, there is no forced change of the PDV modes. However, analysis of single model ensemble, where the mean-state trend cannot be cleanly identified, suggests an apparent anthropogenic change in NPGO decadal variability. This suggests that observed PDV responses to anthropogenic forcing may be erroneously convolved with the background trend pattern. Therefore, correctly determining the mean-state trend is a necessary precursor for identifying forced changes to PDV.

Plain Language Summary

Pacific decadal variability (PDV), characterized by long-term shifts in Pacific sea surface temperatures (SSTs), plays a crucial role in global climate dynamics. Disentangling the influence of human-induced forcing from natural PDV is complicated by their similar temporal scales. Through large ensembles of single-forcing climate model simulations, we demonstrate that anthropogenic forcing predominantly drives spatially heterogeneous mean-state alterations in North Pacific SSTs, which align with the primary PDV patterns, including the Pacific Decadal Oscillation (PDO) and North Pacific Gyre Oscillation (NPGO). While the ensemble mean reveals no direct forced changes in PDV modes, individual model realizations indicate an apparent anthropogenic modification of NPGO variability. This suggests that observed PDV responses may conflate anthropogenic trends with natural variability, underscoring the importance of accurately determining mean-state SST trends to isolate and identify forced changes in PDV.

1 Introduction

Pacific decadal variability (PDV) impacts global climate and ecosystems, affecting phenomena such as the recent global warming hiatus (Johnson et al., 2020; Trenberth, 2015; Trenberth & Fasullo, 2013), Northeast Pacific marine heat wave properties (Capotondi et al., 2022; Di Lorenzo & Mantua, 2016), and North American precipitation patterns (B. Dong et al., 2018; L. Dong et al., 2021). PDV is tightly coupled with the most important mode of interannual climate variability in the tropical Pacific, the El Niño Southern Oscillation (ENSO; e.g., Power et al., 2021 and Capotondi et al., 2023), and can be expected to modulate its characteristics and impacts. Understanding PDV's sensitivity to anthropogenic influences is therefore critically important to understand, simulate, and predict in the context of a changing climate.

Numerous studies have suggested that anthropogenic greenhouse gas (GHG) and aerosol emissions may alter PDV. For instance, 21st century PDV intensification has been attributed to GHG-driven enhancements of thermodynamic coupling (Liguori & Di Lorenzo, 2018). Additionally, the increased ocean stratification expected in a warmer climate (Capotondi et al., 2012) may accelerate the ocean adjustment processes central to PDV (Capotondi et al., 2023), leading to faster and weaker decadal variations (Geng et al., 2019). Anthropogenic aerosols have also been shown to affect PDV by inducing cooling in the central North Pacific typical of a positive PDO phase (Hua et al., 2018; Qin et al., 2020) or contributing to negative PDO phases over the past decades (Dittus et al., 2021; Dow et al., 2021; Smith et al., 2016). Conversely, some studies argue that anthropogenic forcing has minimal impact on the observed PDO compared with internal variability (Boo et al., 2015; Newman et al., 2016). These conflicting findings highlight significant uncertainties in the net effect of anthropogenic forcing on Pacific climate variability, which we aim to resolve in this paper.

A major challenge in identifying the response of PDV to anthropogenic influences lies in separating PDV from forced mean state changes. Climate models tend to simulate an evolving warming pattern due to GHGs, especially in the tropics and North Pacific (Andrews et al., 2015; Deser, Phillips, et al., 2020; Xie et al., 2010). While anthropogenic aerosols tend to produce a more heterogeneous hemispheric cooling (Deser, Phillips, et al., 2020; Shi et al., 2022; Wang et al., 2016) and long-term La Niña-like cooling in the tropical Pacific (Hwang et al., 2024). Since the signatures of GHG and aerosol-driven changes are significant in the North Pacific (Huang & Stevenson, 2021; Shi et al., 2022), background trends have the potential to overlap with PDV patterns. Nonlinear temporal changes in mean state responses further complicate the isolation of PDV from background climate trends (Alexander et al., 2018; Solomon et al., 2011; Xu et al., 2022).

The choice of diagnostics used to determine mean-state trends and PDV affects the degree to which they can be separated from one another. The traditional definition of the Pacific Decadal Oscillation (PDO; Mantua et al., 1997) removes the global-mean sea surface temperature (GMSST) to account for temporal mean state changes. While this approach accounts for temporal changes in the mean state, particularly those driven by anthropogenic aerosols, spatially heterogeneous changes in the mean state remain embedded in the variability. Alternatively, removing linear trends fails to capture nonlinear mean state variations (e.g., Xu et al., 2022). These limitations make it difficult to assess anthropogenic influences on PDV using observations or single model realizations.

Large ensemble simulations using coupled climate models offer a solution by enabling the separation of forced mean state changes from internal variability. These are suites of typically 20-100 simulations with a single climate model, subject to the same external forcing (e.g. Deser, Phillips, et al., 2020; Lehner et al., 2020; Maher et al., 2021), but differing only in their initial conditions.. Averaging all ensemble members provides a statistically robust estimate of the response due to external forcing, which can then be removed from each ensemble member to leave representations of different realizations of internal variability, as demonstrated in studies detecting changes of marine heatwave (Alexander et al., 2018; Deser et al., 2024), North American precipitation (Deser et al., 2014), and future ENSO behavior (Maher et al., 2023). This approach facilitates isolating uncertainty from internal variability, enabling clearer comparisons of different PDV metrics and improving our understanding of PDV's forced response.

2 Data and Methods

2.1 CESM and CMIP6 Large Ensemble Simulations

This study employs large ensemble simulations from the National Center for Atmospheric Research Community Earth System Model version 2 (CESM2; Danabasoglu et al., 2020) covering the historical period (1850-2015), which includes both natural and anthropogenic climate forcings (hereafter “full-forcing” simulations). The CESM2 full-forcing Large Ensemble (CESM2-LE; Rodgers et al., 2021) contains 50 ensemble members with smoothed biomass burning (smbb), and 50 members which do not employ smoothing. Here the smbb ensembles are used to reduce spurious influences from discontinuities in biomass burning emissions at the start and end of the satellite era (1997-2014; Fasullo et al., 2022). Each ensemble member has unique atmospheric and oceanic initial conditions based on the phase of the Atlantic meridional overturning circulation in the pre-industrial control simulation (Rodgers et al., 2021).

To isolate the impact of anthropogenic emissions on PDV, we also analyze experiments from the CESM2 single-forcing large ensemble (Simpson et al., 2023), mainly focusing on GHG and anthropogenic aerosols (AAER) (Table S1). These single-forcing large ensembles were constructed using an “only-one” approach (Simpson et al., 2023), where only the target forcing evolves through time while others are fixed at 1850 levels. The CESM2 SF-LE also contains biomass burning-only and “everything else” simulations, but we exclude these from the present analysis as our focus is on GHG and aerosols.

To ensure the robustness of our CESM results, we also analyze the CESM1 Large Ensemble (Kay et al., 2015) and CESM1 single-forcing large ensemble (Deser, Phillips, et al., 2020), details for which are provided in the supplementary (Text S1). Additionally, Coupled Model Intercomparison Project Phase 6 (CMIP6)-class models with large ensemble sizes (≥10 members) are included. This resulted in the selection of an additional eight climate models covering the same study period (1920-2015). This includes two recently generated large ensembles using the Energy Exascale Earth System Model versions 1 (E3SMv1; Stevenson et al., 2023) and version 2 (E3SMv2; Fasullo et al., 2024) and six other CMIP6-class large ensembles (ACCESS-ESM1-5, CanESM5, GFDL-SPEAR-MED, IPSL-CM6A-LR, MIROC6, MIROC-ES2L) from various modeling centers, taken from an existing compilation of large ensemble climate information (Brunner et al., 2020; Maher et al., 2023). The CMIP6 model names and their ensemble sizes are summarized in Table S2.

2.2 Diagnosis of Pacific Modes Independent of the Forced Mean State

To disentangle the slow spatiotemporal evolution of the mean state from internal variability in climate models, we utilize three statistical methods. This allows us to assess how the choice of diagnostic used to identify PDV affect the conclusions drawn about forced changes in PDV – and the ability of observations to provide definitive answers.

2.2.1 Traditional method

The first approach allows us to characterize internal variability using definitions traditionally applied to observations. This method also provides the ability to directly compare model- and observationally based results. Here we adopt a conventional PDV definition used in the literature (Mantua et al., 1997; Newman et al., 2016; Trenberth & Fasullo, 2013) by removing the GMSST. SST anomalies (SSTA) are defined as deviations from the annual cycle after removal of the GMSST removal, to minimize the influence of forced mean state changes.

PDV modes are then calculated by applying empirical orthogonal function (EOF) analysis to SSTA over the North Pacific (20°N-70°N, 110°E-70°W) in each individual ensemble member (or observations). We include the two leading EOF modes of SST variability, where the leading EOF describes the PDO (Mantua et al., 1997), and the second EOF mode identifies the North Pacific Gyre Oscillation (NPGO; Di Lorenzo et al., 2008).

2.2.2 'Projection'

The traditional method assumes that removing the time series of global-mean SST is sufficient to remove the mean-state trend from PDV. However, anthropogenic forcings may also change the underlying structure of PDV. The projection method is a way of detecting this effect; it relies on identifying fixed modes of variability using a preindustrial control simulation, which are then projected onto the forced simulation (e.g., Maher et al., 2014).

First, we calculate the two leading EOF modes of monthly SSTA in the North Pacific (20°N-70°N, 110°E-70°W) from preindustrial control simulations without any impact of anthropogenic forcing. Historical SSTA from forced simulations are then projected onto these preindustrial EOF patterns at each timestep to obtain a time series of projection coefficients, which are regressed against global SSTA in the historical runs to identify the temporal behavior of PDV patterns.

2.2.3 'Ensemble Mean Removed'

Simply removing GMSST from individual simulations may not fully capture spatial SST structures affected by anthropogenic forcing. The projection method can still introduce mean-state biases if forced changes align with variability patterns. Utilizing large ensemble simulations, we can robustly characterize the forced changes in the mean, including spatial structure information, and distinguish those from changes in variability (Deser, Lehner, et al., 2020; Lehner et al., 2020; Maher et al., 2021).

In the 'ensemble mean removed' method, we first compute the ensemble mean SST at each grid point for each month and subtract it from each ensemble member to eliminate forced mean state changes. After removing the ensemble mean, we calculate the anomalies by subtracting the monthly climatology over the study period (1920-2014). EOF analysis is then performed on the residual SSTA within the same North Pacific domain to extract the PDV modes. The fractions of variance explained by each method are summarized in Table S3.

2.3 Metrics Using Ensemble Mean to Represent Forced Mean State Changes

External forcings, especially anthropogenic aerosols, have varied non-monotonically over the historical period. In the case of aerosols, this is due to changing regional emission policies, with sulfate aerosol emissions increasing before the 1980s and slightly declining afterward (Simpson et al., 2023). To visually represent the time-evolving forced SST mean state changes after GMSST removed from GHG and aerosol forcings, we extract the first EOF mode from GHG (explaining 74.9% of variance) and aerosol simulations (explaining 83.2% of variance) over the North Pacific domain (20°N-70°N, 110°E-70°W). Similar results are observed for the global domain. The combined impact of GHGs and aerosols is represented by adding the individual mean state impacts of GHGs and aerosols together.

3 Results

3.1 GHG and Aerosol Effects on Pacific Decadal Variability

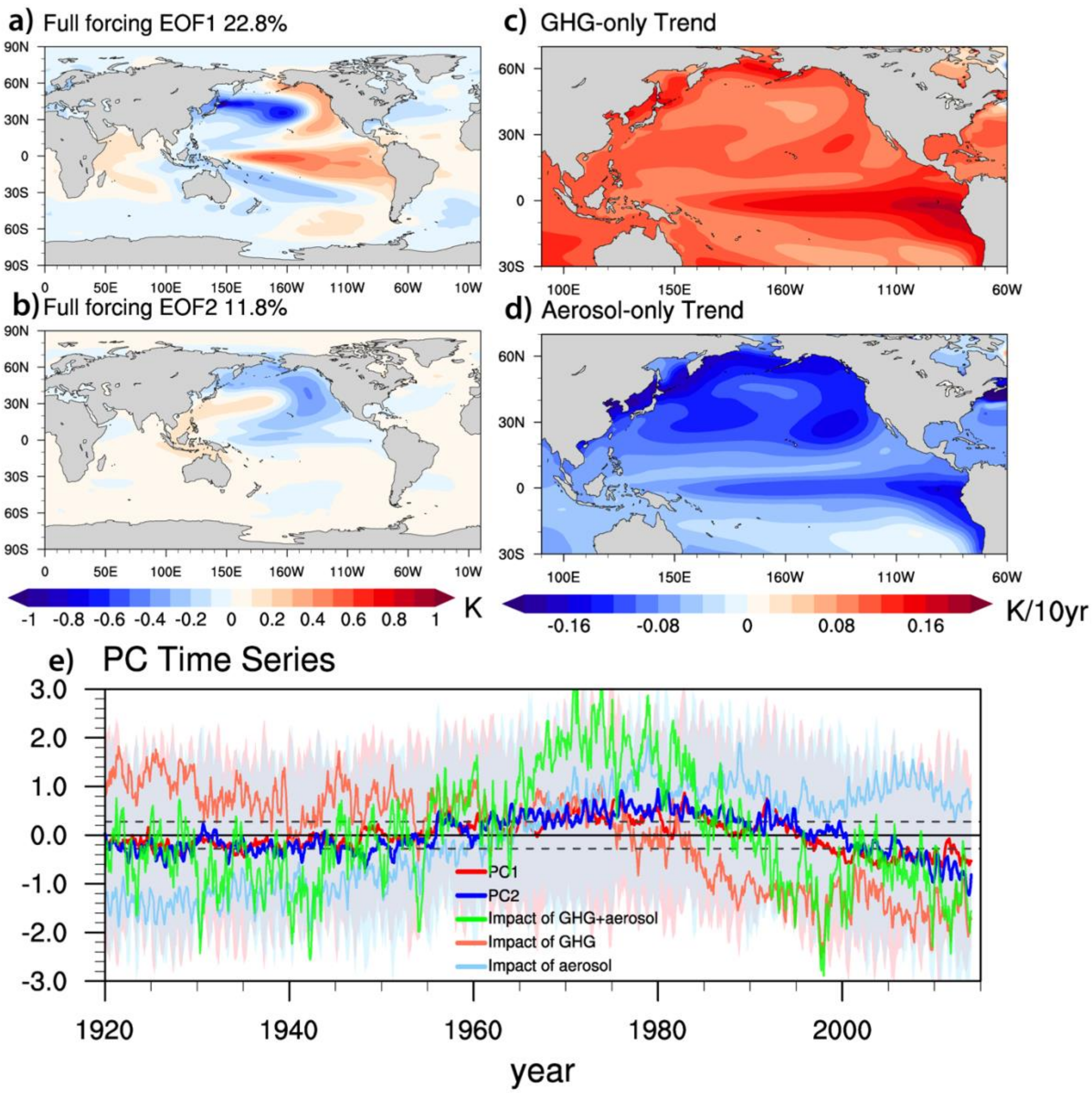

Figure 1. PDO and NPGO-like modes in CESM2, calculated using the traditional method, and compared with anthropogenic forcing patterns. a), b): Ensemble mean regression of SSTA onto

the first and second EOF modes calculated using the traditional method (Section 2.2.1). The ensemble mean variance fractions explained by each mode are shown at the top. c), d): Linear trend of Pacific SSTA in CESM2 GHG and aerosol single-forcing simulations (1920-2014) (units: K/10-years). e): The time series of the mean state changes for GHG-only (orange) and aerosol-only (cyan) forcings represented by the PC1 of the SST ensemble mean after GMSST removed (see Section 2.3; the corresponding EOF patterns are shown in Fig. S1). The combined impact of these forcings is shown by the green line. Also shown are PC1 (red) and PC2 (blue) time series of PDV from CESM2-LE, with shading for two standard deviations among ensemble members and gray dashed lines indicating 2.5% and 97.5% confidence bounds from 10,000 bootstrap samples.

We evaluate PDV performance in CESM2-LE using the traditional definition, which removes the GMSST to separate PDV from mean state changes. The leading mode in the CESM2-LE full-forcing simulations (Fig. 1a) resembles the PDO pattern in NOAA Extended Reconstructed SST V5 (ERSSTv5; Fig. S2; pattern correlation of 0.94), showing cooling centered around the Kuroshio-Oyashio Extension region and warming along the North American coast and in the tropical Pacific. However, the simulated PDO pattern exhibits a westward shift bias, common among CMIP5/6 models (e.g., Fasullo et al., 2020), possibly due to the underestimation of tropical-extratropical interactions (Zhao et al., 2021). The second mode in CESM2 resembles the NPGO (pattern correlation of 0.82), again with slightly stronger cold SSTA in the tropics compared to observations (Figs. 1b & S2b).

The long-term response of the two PDV modes in CESM2—the PDO-like and NPGO-like—aligns with the reversed evolution of anthropogenic forcing. The PC1 ensemble mean shows a positive trend from 1950 to 1980, followed by a negative trend toward a negative PDO phase from 1980 to 2014 (Fig. 1e), consistent with the combined effects of GHG and aerosol forcing (Fig. 1e). The impact of GHG and aerosol forcing on the mean state is assessed through the leading mode of ensemble-mean SST variability in the CESM2 single-forcing simulations (Fig. S1). Overall, GHG-induced warming tends to exert a negative influence on PDV, while anthropogenic aerosols have a contrasting, positive effect (Figs. 1b & 1c). Importantly, although the mean value of the PC coefficients changes through time, the variance associated with both PDV modes are not appreciably changing over time (Fig. S3). This suggests that the effects of forcing are primarily felt through changes in the phase of PDV – at least, as diagnosed using the traditional method.

The PC1 time series in the CESM2 GHG and aerosol single-forcing simulations shows no significant long-term changes under the traditional definition (Fig. S4). In contrast, the second mode exhibits a long-term response, particularly a positive trend in aerosol-only simulations (Fig. S4). The muted response of the PDO-like PC1 in the GHG and aerosol simulations can be attributed to the spatial pattern of the forced mean state response: SST changes from GHGs are prominent in the tropical Pacific (Fig. S1), while aerosol impacts are large in both the tropical and North Pacific (Fig. S1). These influences are unlikely to affect the PDO pattern, which features opposite signs between the tropics and extratropics (Fig. 1a). No significant contribution from biomass burning or other natural forcings in the CESM2 biomass and everything-else simulations (figure not shown). Therefore, the long-term PDO response in the CESM2 full-forcing simulation (Fig. 1e) may perhaps result from a nonlinear interaction between GHG and aerosols or a key process is missing in model. However, the single-forcing ensembles indicate that the PDO is little affected by either forcing while the NPGO appears to undergo an amplitude increase primarily due to aerosol forcing.

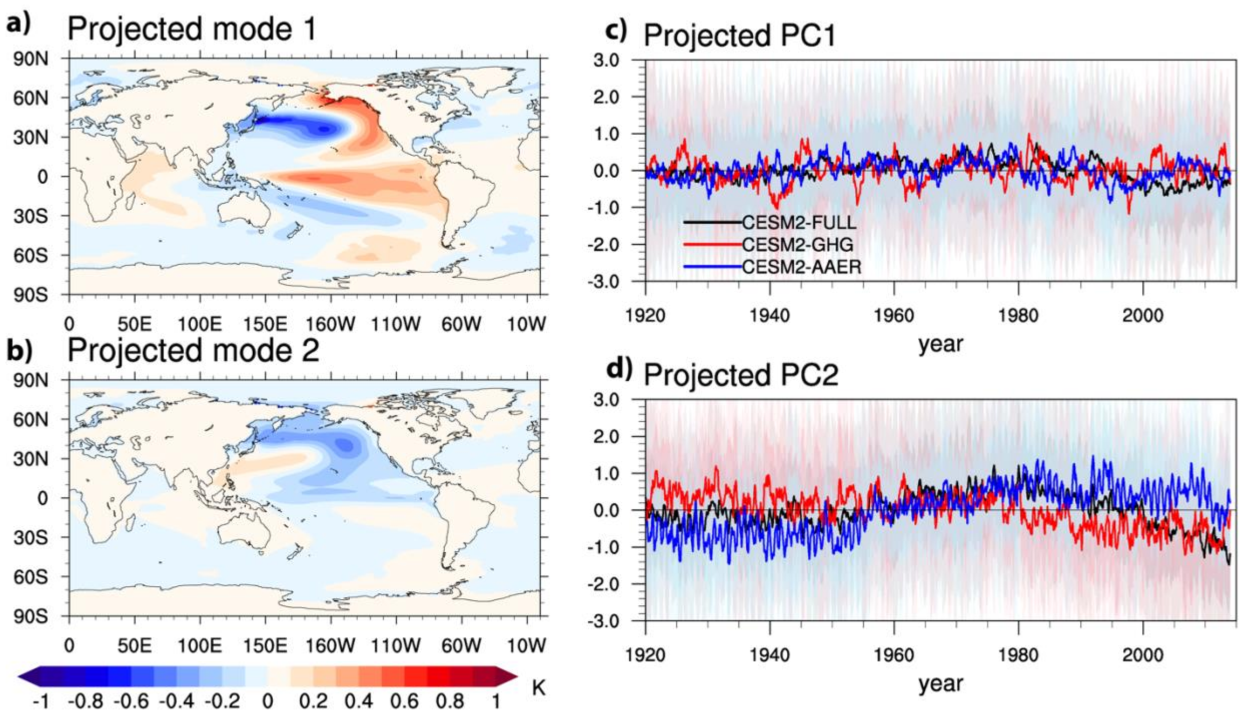

Figure 2. PDO and NPGO-like modes in CESM2, calculated using the projection method. a), b): Ensemble mean regression of SST onto the projected time series of the first and second modes computed from the CESM2 preindustrial control run (Fig. S5). c), d): Time series of the 'projection' modes 1 and 2 from CESM2 LE full-forcing (black), GHG-only (red), and aerosol-only (blue) simulations. Dark (light) shading represents one (two) standard deviation(s), while solid lines show ensemble means.

Since the traditional definition over the historical period may not completely eliminate anthropogenic influences, we revisit the problem by using fixed patterns of internal variability derived from the CESM2 preindustrial control run (the "projection method"). Fields from the forced CESM2 simulations are projected onto these fixed modes (Section 2.2.2) to track the evolution of these patterns in a changing climate. The two leading North Pacific modes in the control run resemble PDO-like and NPGO-like patterns (Fig. S5).

The PC time series through the projection method are consistent with the traditional method: through the 'projection' definition in CESM2, the "PDO" mode (PC1; Fig. 2a) shows weak long-term changes in the full-forcing simulations, with no significant responses to GHG or aerosols (Fig. 2c). In contrast, the second 'projection' mode ("NPGO"; Fig. 2b) exhibits a larger forced signal, especially post-1950 (Fig. 2d). Anthropogenic aerosol emission-driven mean state changes (Fig. 1e) are responsible for the positive phase of the NPGO mode around 1950-1990, persisting until the end of the AAER simulations (Fig. 2d). Aerosol effects are also apparent in the full-forcing simulation, with a positive phase change in the mid-20th century (Fig. 2d). However, after 1990, increasing GHG and reduced aerosol emissions lead to a negative trend in the full-forcing 'projection' mode 2 (Fig. 2d).

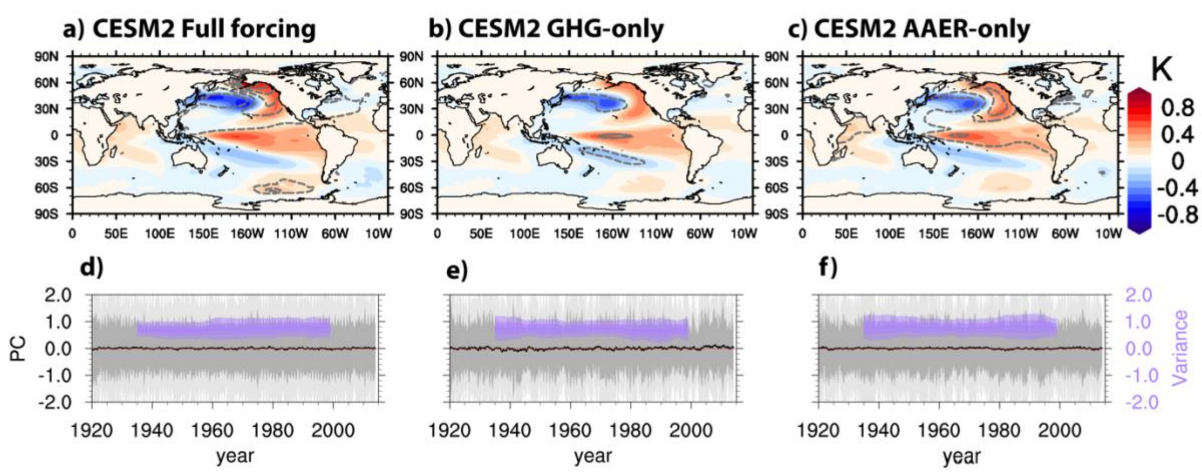

Figure 3. PDO-like modes in CESM2 full and single-forcing ensembles, calculated using the 'ensemble mean removed' method. a), c), e): Ensemble mean of regression pattern of the first SSTA EOF mode for the CESM2 full-forcing, GHG-only, and AAER-only simulations after removing the ensemble mean at each grid point. Contours show differences between traditional and 'ensemble mean removed' PDV modes, with solid (dashed) contours for positive (negative) anomalies and a contour interval of 0.05K. b), d), f): PC1 time series for the leading mode in full-forcing, GHG-only, and AAER-only simulations. Purple lines show 30-year moving

variance, with dark (light) shading representing one (two) standard deviation(s), and solid lines showing ensemble means.

The preceding analyses suggest that anthropogenic forcing has the potential to influence PDV through long-term mean state changes, but in both the traditional and projection methods, the background mean state trend is not fully separated from changes to the nature of PDV itself. Using large ensemble simulations to capture the mean state response, we can effectively capture the time-varying forced response in climate models by removing the ensemble mean (the 'ensemble mean removed' method, see Section 2.2.3). The leading EOF mode then shows no significant trend or variance changes in the full-forcing (Fig. 3b), GHG (Fig. 3d), or aerosol (Fig. 3f) single-forcing ensembles. The same holds for the second, NPGO-like mode (Fig. S6). Additionally, there is no detectable change in the 30-year moving variance of either mode (Figs. 3d-f & S6), indicating that PDO variability is unaffected by anthropogenic forcing.

The robustness of these results is confirmed through comparison with large ensembles from 9 other climate models (Tables S1, S2, Text S2). In most models, externally forced mean state changes tend to cause a response in the dominant (PDO-like) mode similar to CESM2, with a positive phase in the 1980s and a subsequent negative trend (Fig. S11) for the traditional and projection methods. However, in all models the ensemble mean removed method results in a near-complete removal of trends in the PDO; this suggests that the mean-state influence is generally the dominant factor in PDO phase shifts. The same is true for the second (NPGO-like) mode, where the ensemble mean removed method eliminates trends in PC2 (Fig. S12). However, there is more diversity in the behavior of the NPGO-like mode, both in terms of spatial pattern (not pictured) and temporal behavior (Fig. S12); this may potentially relate to differences in aerosol representation and aerosol-cloud interactions across models.

3.2 Comparison with Observed Pacific Modes

The inconsistent response of the PDO and NPGO to forcing across models, and the influence of the mean-state trend on PDV diagnosed using methods appropriate for observations, raises questions regarding the true sensitivity of decadal Pacific climate variability to forcing. Models are known to have limitations in representing tropical Pacific trends (Wills et al., 2022), which implies that simulated PDV may also be affected when using the traditional diagnostic method.

To investigate the realism of PDO/NPGO responses, we compare CESM2-LE results with observations in Figure 4.

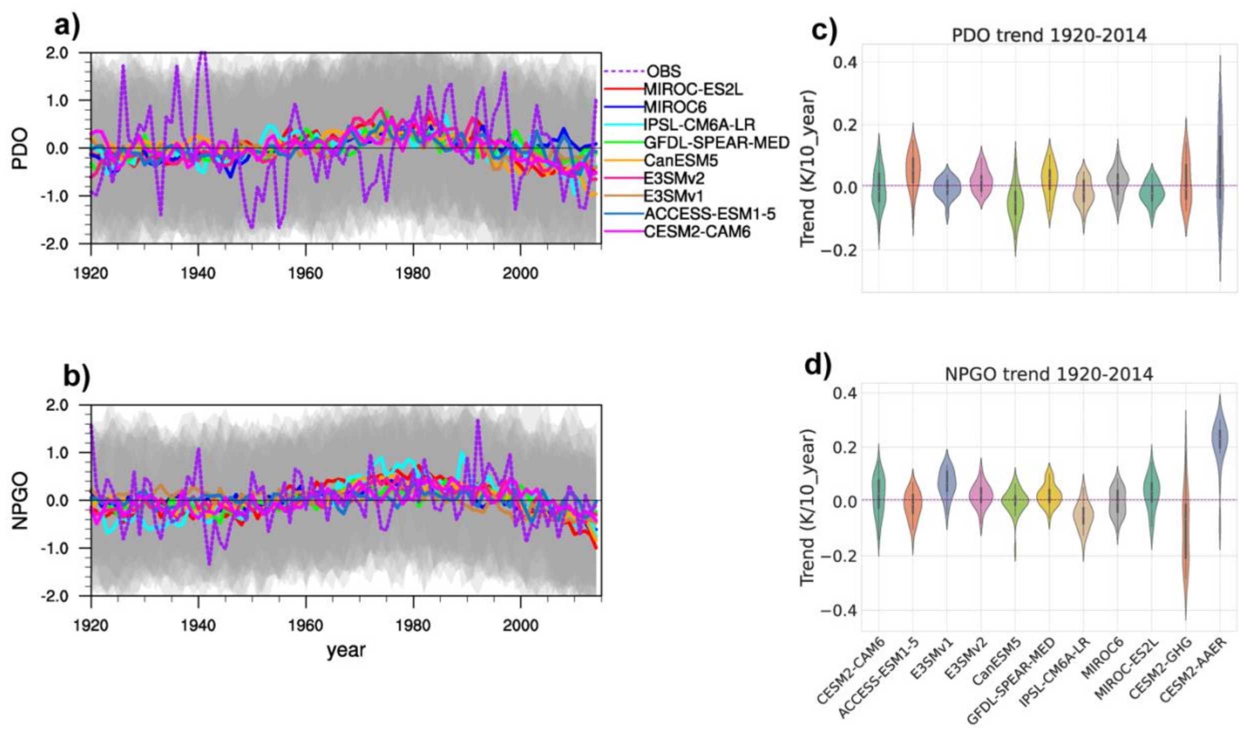

Figure 4. Time series and long-term trend of PDO and NPGO index in CESM2 as compared with observations, using the traditional method. a), b): Time series of PDO-like and NPGO-like modes from CMIP6 large ensembles and observations (ERSSTv5). Shading indicates two standard deviations of ensemble spread, while solid lines represent ensemble means. c), d): Linear trend magnitudes in PDO-like and NPGO-like modes over 1920-2014 in CMIP6 and CESM2 single-forcing simulations. Purple dashed lines in violin plots represent observational trends.

The observed PDO was in the positive phase during ~1925-1945 and 1980-2000, and the negative phase during 1945-1979 and 2000-2014 (Newman et al., 2016). Previous studies have linked observed PDO phase changes to aerosols (Dittus et al., 2021; Dow et al., 2021; Smith et al., 2016) or a combination of GHG and aerosol emissions (L. Dong et al., 2014). However, estimates of the forced response using the traditional method (Fig. 4a) do not align temporally with the observed PDO in any model examined, suggesting that observed phase changes are more likely a result of internal variability. Consistent with this finding, the long-term PDO trend remains near zero in CESM2, most of CMIP6 large ensembles and observations (Fig. 4c).

During the historical period (1920-2014), the NPGO index shows no significant linear trend in both CESM2 full-forcing simulations and observations (Fig. 4d). With exceptions in some CMIP6 large ensembles: a weak positive trend (e.g., E3SMv1); a weak negative trend (e.g., IPSL-CAM6A-LR). In CESM2, this appears to result from compensation between GHG and aerosol forcing (Fig 4d), indicating the need to correctly represent mean-state responses to both forcings. We note that these results are somewhat sensitive to the detrending method used (Brown et al., 2015). Using quadratic detrending instead of GMSST removal before EOF analysis aligned the observed NPGO more closely with CESM2 (Fig. S13), but the long-term trend in both cases is near zero.

4 Conclusions

PDV plays a pivotal role in modulating climate over the Pacific Ocean and impacting global climate. Accurately understanding the influence of anthropogenic forcing on PDV is therefore essential for reliable predictions of decadal variability and trends. However, externally forced mean state changes may become intertwined with the PDV response, leaving the relationship between PDV and external forcing unclear. This study employs three diagnostic approaches—the “traditional”, “projection”, and “ensemble mean removed”—to disentangle mean state changes from decadal variability using climate large ensembles.

Consistent with observational findings, a PDO-like mode and an NPGO-like mode are the two major PDV modes in CESM2 as well as other climate models. The PDO shows no significant response to historical forcing in any diagnostic examined; however, the NPGO-like mode does respond to forcing, with aerosols driving a positive trend from 1950 to 1980 and GHGs inducing a negative shift from 1980 to 2014. The magnitude of the apparent forced response in the NPGO mode, however, depends sensitively on the method of mean-state removal. When the ensemble mean is removed, neither the PDO or NPGO respond to forcing; as this is the most statistically robust method, this indicates that commonly used observational diagnostics are affected by mean-state trends.

Our results offer a potential path toward resolving the differing responses to the PDO reported in other studies. Although aerosol forcing drives mean-state trends which project onto the PDO mode (e.g., Dittus et al., 2021), the robust lack of overall PDO response to forcing suggests that observed PDO phase changes may simply reflect internal climate variability. The major response of decadal climate variability to aerosols appears to be in the second, NPGO-like mode; however, even for the NPGO mode, the dominant cause of the apparent response is the projection of the mean-state trend onto the spatial pattern of the NPGO rather than a true change in the nature of NPGO variability itself. It is also crucial to note that in all PDV diagnostics which can be applied to observations (e.g. those which do not involve averaging many realizations of internal variability), the effect of the mean state is not fully removed from the NPGO-like mode. This implies that accurately simulating North Pacific mean-state trends in climate models is crucial for interpreting disagreements between simulated and observed PDV – and, in turn, ensuring a realistic representation of the PDV response to anthropogenic forcing.

Acknowledgments

CX and SS were supported by the U.S. Department of Energy, DE-SC0019418. SS was also supported by NSF CAREER, OCE-2142953. AC was supported by the NOAA Climate Program Office Climate Variability and Predictability Program and by DOE Award DE-SC0023228. NM was supported by the Australian Research Council Discovery Early Career Researcher Award DE230100315. JF were supported by NASA Awards 80NSSC21K1191, 80NSSC17K0565, and 80NSSC22K0046, and by the Regional and Global Model Analysis (RGMA) component of the Earth and Environmental System Modeling Program of the U.S. Department of Energy's Office of Biological & Environmental Research (BER) under Award Number DE-SC0022070, as well as NSF Award 2103843. We appreciate the assistance of Dr. Youngji Joh. We would like to acknowledge high-performance computing support from Cheyenne (doi:10.5065/D6RX99HX) and Derecho (https://doi.org/10.5065/qx9a-pg09) provided by NCAR's Computational and Information Systems Laboratory, sponsored by the National Science Foundation. We also acknowledge the Community Earth System Model working groups.

Data Availability Statement

The CESM2 full-forcing large ensemble (Danabasoglu et al., 2020; Rodgers et al., 2021) is accessible at https://www.cesm.ucar.edu/community-projects/lens2/data-sets, while the CESM2 single-forcing large ensemble (Simpson et al., 2023) can be found https://www.cesm.ucar.edu/working-groups/climate/simulations/cesm2-single-forcing-le. The CESM1 large ensemble (Kay et al., 2015) is available https://www.cesm.ucar.edu/community-projects/lens/data-sets, and the CESM1 all-but-one simulation (Deser, Phillips, et al., 2020) can be accessed https://www.cesm.ucar.edu/working-groups/climate/simulations/cesm1-single-forcing-le. CMIP6 large ensembles used in this study are detailed in Table S2, with the data available at https://aims2.llnl.gov/search/cmip6/. NOAA Extended Reconstructed SST V5 (ERSSTv5; Huang et al., 2017) can be downloaded through https://psl.noaa.gov/data/gridded/data.noaa.ersst.v5.html.

References

Alexander, M. A., Scott, J. D., Friedland, K. D., Mills, K. E., Nye, J. A., Pershing, A. J., & Thomas, A. C. (2018). Projected sea surface temperatures over the 21st century: Changes in the mean, variability and extremes for large marine ecosystem regions of Northern Oceans. Elementa: Science of the Anthropocene, 6, 9. https://doi.org/10.1525/elementa.191

Andrews, T., Gregory, J. M., & Webb, M. J. (2015). The Dependence of Radiative Forcing and Feedback on Evolving Patterns of Surface Temperature Change in Climate Models. Journal of Climate, 28(4), 1630–1648. https://doi.org/10.1175/JCLI-D-14-00545.1

Boo, K.-O., Booth, B. B. B., Byun, Y.-H., Lee, J., Cho, C., Shim, S., & Kim, K.-T. (2015). Influence of aerosols in multidecadal SST variability simulations over the North Pacific. Journal of Geophysical Research: Atmospheres, 120(2), 517–531. https://doi.org/10/ghhwd7

Brown, P. T., Li, W., & Xie, S.-P. (2015). Regions of significant influence on unforced global mean surface air temperature variability in climate models. Journal of Geophysical Research: Atmospheres, 120(2), 480–494. https://doi.org/10.1002/2014JD022576

Brunner, L., Hauser, M., Lorenz, R., & Beyerle, U. (2020). The ETH Zurich CMIP6 next generation archive: technical documentation. https://doi.org/10.5281/zenodo.3734128

Capotondi, A., Newman, M., Xu, T., & Di Lorenzo, E. (2022). An Optimal Precursor of Northeast Pacific Marine Heatwaves and Central Pacific El Niño Events. Geophysical Research Letters, 49(5), e2021GL097350. https://doi.org/10.1029/2021GL097350

Capotondi, A., Alexander, M. A., Bond, N. A., Curchitser, E. N., & Scott, J. D. (2012). Enhanced upper ocean stratification with climate change in the CMIP3 models. Journal of Geophysical Research: Oceans, 117(C4). https://doi.org/10.1029/2011JC007409

Capotondi, A., McGregor, S., McPhaden, M. J., Cravatte, S., Holbrook, N. J., Imada, Y., et al. (2023). Mechanisms of tropical Pacific decadal variability. Nature Reviews Earth & Environment, 4(11), 754–769. https://doi.org/10.1038/s43017-023-00486-x

Danabasoglu, G., Lamarque, J. -F., Bacmeister, J., Bailey, D. A., DuVivier, A. K., Edwards, J., et al. (2020). The Community Earth System Model Version 2 (CESM2). Journal of Advances in Modeling Earth Systems, 12(2), e2019MS001916. https://doi.org/10.1029/2019MS001916

Deser, C., Lehner, F., Rodgers, K. B., Ault, T., Delworth, T. L., DiNezio, P. N., et al. (2020). Insights from Earth system model initial-condition large ensembles and future prospects. Nature Climate Change, 10(4), 277–286. https://doi.org/10.1038/s41558-020-0731-2

Deser, C., Phillips, A. S., Alexander, M. A., & Smoliak, B. V. (2014). Projecting North American Climate over the Next 50 Years: Uncertainty due to Internal Variability. Journal of Climate, 27(6), 2271–2296. https://doi.org/10.1175/JCLI-D-13-00451.1

Deser, C., Phillips, A. S., Simpson, I. R., Rosenbloom, N., Coleman, D., Lehner, F., et al. (2020). Isolating the Evolving Contributions of Anthropogenic Aerosols and Greenhouse Gases: A New CESM1 Large Ensemble Community Resource. Journal of Climate, 33(18), 7835–7858. https://doi.org/10/ghwh37

Deser, C., Phillips, A. S., Alexander, M. A., Amaya, D. J., Capotondi, A., Jacox, M. G., & Scott, J. D. (2024). Future Changes in the Intensity and Duration of Marine Heat and Cold Waves: Insights from Coupled Model Initial-Condition Large Ensembles. Journal of Climate, 37(6), 1877–1902. https://doi.org/10.1175/JCLI-D-23-0278.1

Di Lorenzo, E., & Mantua, N. (2016). Multi-year persistence of the 2014/15 North Pacific marine heatwave. Nature Climate Change, 6(11), 1042–1047. https://doi.org/10/f9dn63

Di Lorenzo, E., Schneider, N., Cobb, K. M., Franks, P. J. S., Chhak, K., Miller, A. J., et al. (2008). North Pacific Gyre Oscillation links ocean climate and ecosystem change. Geophysical Research Letters, 35(8), L08607. https://doi.org/10/dtnn2s

Dittus, A. J., Hawkins, E., Robson, J. I., Smith, D. M., & Wilcox, L. J. (2021). Drivers of Recent North Pacific Decadal Variability: The Role of Aerosol Forcing. Earth’s Future, 9(12), e2021EF002249. https://doi.org/10.1029/2021EF002249

Dong, B., Dai, A., Vuille, M., & Timm, O. E. (2018). Asymmetric Modulation of ENSO Teleconnections by the Interdecadal Pacific Oscillation. Journal of Climate, 31(18), 7337–7361. https://doi.org/10.1175/jcli-d-17-0663.1

Dong, L., Zhou, T., & Chen, X. (2014). Changes of Pacific decadal variability in the twentieth century driven by internal variability, greenhouse gases, and aerosols. Geophysical Research Letters, 41(23), 8570–8577. https://doi.org/10/f6ww5k

Dong, L., Leung, L. R., Song, F., & Lu, J. (2021). Uncertainty in El Niño-like warming and California precipitation changes linked by the Interdecadal Pacific Oscillation. Nature Communications, 12(1), 6484. https://doi.org/10/gnn5pv

Dow, W. J., Maycock, A. C., Lofverstrom, M., & Smith, C. J. (2021). The Effect of Anthropogenic Aerosols on the Aleutian Low. Journal of Climate, 34(5), 1725–1741. https://doi.org/10/gh4mf4

Fasullo, J. T., Phillips, A. S., & Deser, C. (2020). Evaluation of Leading Modes of Climate Variability in the CMIP Archives. Journal of Climate, 33(13), 5527–5545. https://doi.org/10.1175/JCLI-D-19-1024.1

Fasullo, J. T., Lamarque, J.-F., Hannay, C., Rosenbloom, N., Tilmes, S., DeRepentigny, P., et al. (2022). Spurious Late Historical-Era Warming in CESM2 Driven by Prescribed Biomass Burning Emissions. Geophysical Research Letters, 49(2), e2021GL097420. https://doi.org/10.1029/2021GL097420

Fasullo, J. T., Golaz, J.-C., Caron, J. M., Rosenbloom, N., Meehl, G. A., Strand, W., et al. (2024). An overview of the E3SM version 2 large ensemble and comparison to other E3SM and CESM large ensembles. Earth System Dynamics, 15(2), 367–386. https://doi.org/10.5194/esd-15-367-2024

Geng, T., Yang, Y., & Wu, L. (2019). On the Mechanisms of Pacific Decadal Oscillation Modulation in a Warming Climate. Journal of Climate, 32(5), 1443–1459. https://doi.org/10/gjf2xr

Hua, W., Dai, A., & Qin, M. (2018). Contributions of Internal Variability and External Forcing to the Recent Pacific Decadal Variations. Geophysical Research Letters, 45(14), 7084–7092. https://doi.org/10.1029/2018gl079033

Huang, B. Y., Thorne, P. W., Banzon, V. F., Boyer, T., Chepurin, G., Lawrimore, J. H., et al. (2017). Extended Reconstructed Sea Surface Temperature, Version 5 (ERSSTv5): Upgrades, Validations, and Intercomparisons. *Journal of Climate*, *30*(20), 8179–8205. https://doi.org/10.1175/Jcli-D-16-0836.1

Huang, X., & Stevenson, S. (2021). Connections Between Mean North Pacific Circulation and Western US Precipitation Extremes in a Warming Climate. Earth's Future, 9(6), e2020EF001944. https://doi.org/10.1029/2020EF001944

Hwang, Y.-T., Xie, S.-P., Chen, P.-J., Tseng, H.-Y., & Deser, C. (2024). Contribution of anthropogenic aerosols to persistent La Niña-like conditions in the early 21st century. Proceedings of the National Academy of Sciences, 121(5), e2315124121. https://doi.org/10.1073/pnas.2315124121

Johnson, N. C., Amaya, D. J., Ding, Q., Kosaka, Y., Tokinaga, H., & Xie, S.-P. (2020). Multidecadal modulations of key metrics of global climate change. Global and Planetary Change, 188, 103149. https://doi.org/10.1016/j.gloplacha.2020.103149

Kay, J. E., Deser, C., Phillips, A., Mai, A., Hannay, C., Strand, G., et al. (2015). The Community Earth System Model (CESM) Large Ensemble Project: A Community Resource for Studying

Climate Change in the Presence of Internal Climate Variability. Bulletin of the American Meteorological Society, 96(8), 1333–1349. https://doi.org/10.1175/bams-d-13-00255.1

Lehner, F., Deser, C., Maher, N., Marotzke, J., Fischer, E. M., Brunner, L., et al. (2020). Partitioning climate projection uncertainty with multiple large ensembles and CMIP5/6. Earth System Dynamics, 11(2), 491–508. https://doi.org/10.5194/esd-11-491-2020

Liguori, G., & Di Lorenzo, E. (2018). Meridional Modes and Increasing Pacific Decadal Variability Under Anthropogenic Forcing. Geophysical Research Letters, 45(2), 983–991. https://doi.org/10/gc4b3g

Maher, N., Gupta, A. S., & England, M. H. (2014). Drivers of decadal hiatus periods in the 20th and 21st centuries. Geophysical Research Letters, 41(16), 5978–5986. https://doi.org/10.1002/2014gl060527

Maher, N., Milinski, S., & Ludwig, R. (2021). Large ensemble climate model simulations: introduction, overview, and future prospects for utilising multiple types of large ensemble. Earth System Dynamics, 12(2), 401–418. https://doi.org/10.5194/esd-12-401-2021

Maher, N., Wills, R. C. J., DiNezio, P., Klavans, J., Milinski, S., Sanchez, S. C., et al. (2023). The future of the El Niño–Southern Oscillation: using large ensembles to illuminate time-varying responses and inter-model differences. Earth System Dynamics, 14(2), 413–431. https://doi.org/10.5194/esd-14-413-2023

Mantua, N. J., Hare, S. R., Zhang, Y., Wallace, J. M., & Francis, R. C. (1997). A Pacific Interdecadal Climate Oscillation with Impacts on Salmon Production. Bulletin of the American Meteorological Society, 78(6), 1069–1079. https://doi.org/10.1175/1520-0477(1997)078<1069:APICOW>2.0.CO;2

Newman, M., Alexander, M. A., Ault, T. R., Cobb, K. M., Deser, C., Di Lorenzo, E., et al. (2016). The Pacific Decadal Oscillation, Revisited. Journal of Climate, 29(12), 4399–4427. https://doi.org/10/gbpwpp

Power, S., Lengaigne, M., Capotondi, A., Khodri, M., Vialard, J., Jebri, B., et al. (2021). Decadal climate variability in the tropical Pacific: Characteristics, causes, predictability, and prospects. Science, 374(6563), eaay9165. https://doi.org/10.1126/science.aay9165

Qin, M., Dai, A., & Hua, W. (2020). Aerosol-forced multidecadal variations across all ocean basins in models and observations since 1920. Science Advances, 6(29), eabb0425. https://doi.org/10/ghhkk6

Rodgers, K. B., Lee, S.-S., Rosenbloom, N., Timmermann, A., Danabasoglu, G., Deser, C., et al. (2021). Ubiquity of human-induced changes in climate variability. Earth System Dynamics, 12(4), 1393–1411. https://doi.org/10.5194/esd-12-1393-2021

Shi, J.-R., Kwon, Y.-O., & Wijffels, S. E. (2022). Two Distinct Modes of Climate Responses to the Anthropogenic Aerosol Forcing Changes. Journal of Climate, 35(11), 3445–3457. https://doi.org/10.1175/JCLI-D-21-0656.1

Simpson, I. R., Rosenbloom, N., Danabasoglu, G., Deser, C., Yeager, S. G., McCluskey, C. S., et al. (2023). The CESM2 Single-Forcing Large Ensemble and Comparison to CESM1: Implications for Experimental Design. Journal of Climate, 36(17), 5687–5711. https://doi.org/10.1175/JCLI-D-22-0666.1

Smith, D. M., Booth, B. B. B., Dunstone, N. J., Eade, R., Hermanson, L., Jones, G. S., et al. (2016). Role of volcanic and anthropogenic aerosols in the recent global surface warming slowdown. Nature Climate Change, 6(10), 936–940. https://doi.org/10.1038/nclimate3058

Solomon, A., Goddard, L., Kumar, A., Carton, J., Deser, C., Fukumori, I., et al. (2011). Distinguishing the Roles of Natural and Anthropogenically Forced Decadal Climate Variability: Implications for Prediction. Bulletin of the American Meteorological Society, 92(2), 141–156. https://doi.org/10.1175/2010BAMS2962.1

Stevenson, S., Huang, X., Zhao, Y., Di Lorenzo, E., Newman, M., van Roekel, L., et al. (2023). Ensemble Spread Behavior in Coupled Climate Models: Insights From the Energy Exascale Earth System Model Version 1 Large Ensemble. Journal of Advances in Modeling Earth Systems, 15(7), e2023MS003653. https://doi.org/10.1029/2023MS003653

Trenberth, K. E. (2015). Has there been a hiatus? Science, 349(6249), 691–692. https://doi.org/10.1126/science.aac9225

Trenberth, K. E., & Fasullo, J. T. (2013). An apparent hiatus in global warming? Earth's Future, 1(1), 19–32. https://doi.org/10.1002/2013ef000165

Wang, H., Xie, S.-P., & Liu, Q. (2016). Comparison of Climate Response to Anthropogenic Aerosol versus Greenhouse Gas Forcing: Distinct Patterns. Journal of Climate, 29(14), 5175–5188. https://doi.org/10/f8t954

Wills, R. C. J., Dong, Y., Proistosecu, C., Armour, K. C., & Battisti, D. S. (2022). Systematic Climate Model Biases in the Large-Scale Patterns of Recent Sea-Surface Temperature and Sea-Level Pressure Change. Geophysical Research Letters, 49(17), e2022GL100011. https://doi.org/10.1029/2022GL100011

Xie, S.-P., Deser, C., Vecchi, G. A., Ma, J., Teng, H., & Wittenberg, A. T. (2010). Global Warming Pattern Formation: Sea Surface Temperature and Rainfall*. Journal of Climate, 23(4), 966–986. https://doi.org/10.1175/2009JCLI3329.1

Xu, T., Newman, M., Capotondi, A., Stevenson, S., Di Lorenzo, E., & Alexander, M. A. (2022). An increase in marine heatwaves without significant changes in surface ocean temperature variability. Nature Communications, 13(1), 7396. https://doi.org/10.1038/s41467-022-34934-x

Zhao, Y., Lorenzo, E. D., Sun, D., & Stevenson, S. (2021). Tropical Pacific Decadal Variability and ENSO Precursor in CMIP5 Models. Journal of Climate, 34(3), 1023–1045. https://doi.org/10/gh4c6k

Geophysical Research Letters

Supporting Information for

Apparent Changes in Pacific Decadal Variability Caused by Anthropogenically-Induced Mean State Modulations

Chen Xing[1], Samantha Stevenson[1], Emanuele Di Lorenzo[2], Matthew Newman[3], Antonietta Capotondi[3, 4], John Fasullo[5], Nicola Maher[6]

1 Bren School of Environmental Science & Management, University of California at Santa Barbara, Santa Barbara, CA, USA.

2 Department of Earth, Environmental & Planetary Sciences, Brown University, Providence, RI, USA.

3 Physical Sciences Laboratory, NOAA, Boulder, CO, USA.

4 CIRES, University of Colorado at Boulder, Boulder, CO, USA.

5 National Center for Atmospheric Research, Boulder, CO, USA.

6 Research School of Earth Sciences, Australian National University, Canberra, Australian Capital Territory, Australia

Contents of this file

Text S1 to S2
Figures S1 to S13
Tables S1 to S3

Text S1. CESM1 large ensemble and its all-but-one experiments

The CESM1 Large Ensemble (CESM1-LE; Kay et al., 2015) consists of 40 ensemble members spanning 1920 to 2004 with a horizontal resolution of 1° for the atmosphere and land, and a nominal 1° resolution in the ocean (~0.3° near the equator). CESM2 has identical resolution as the CESM1-LE but with updated versions of the constituent models. The ensembles in CESM1-LE are obtained by starting in the same year with a small perturbation in the atmosphere (Kay et al., 2015).

An "all-but-one" configuration is used for the CESM1 single forcing experiments (Deser, Phillips, et al., 2020) where the target forcing is fixed at its 1920 state, while the other forcings vary: these are referred to as the fixed GHG (CESM1-XGHG), the fixed anthropogenic aerosol (CESM1-XAER), and the fixed biomass burning aerosol (CESM1-XBMB) ensembles (Table S1). We analyze monthly data over the 1920-2015 period, excluding the pre-1920 data from CESM2-LE and including a 10-year portion (2006-2015) of the Representative Concentration Pathways (RCP) 8.5 from CESM1-LE.

The effect of each forcing in CESM1 is calculated by taking the ensemble mean difference between the CESM1-LE and the ensemble mean of an all-but-one forcing case (e.g., Touma et al., 2021). For instance, the effect of GHG emissions is computed as

$$\textit{Effect of GHG} = (\textit{CESM1-LE}_i - \textit{CESM1-XGHG}_{em})_{em}$$

Here *i* indicates the i-th ensemble member, and *em* indicates the ensemble mean.

Text S2. Results are consistent across multiple models

The robustness of these results is evaluated by comparison with PDV modes diagnosed using the three analysis methods on other climate models. Specifically, we examine CESM1 full and single forcing large ensembles, as well as 8 large ensembles which participated in CMIP6.

In CESM1, both the full and single-forcing large ensembles also exhibit a "PDO-like" and an "NPGO-like" mode that dominate Pacific variability, whether using the traditional method (Fig. S7) or the 'projection' method (Fig. S8). The major difference in the spatial pattern is that the NPGO pattern in CESM1 is stronger, with more pronounced signals over the Kuroshio extension and warm pool (Fig. S7b), compared to the anomalies in CESM2 (Fig. 1b).

However, unlike the forced signals in CESM2 (Fig. 1e), the PDO or the NPGO modes themselves are mainly dominated by internal variability in full forcing ensembles irrespective of whether the traditional method (Fig. S7c) or the 'projection' method is used (Figs. S8g & S8h). Although anthropogenic aerosols tend to shift the NPGO mode to a positive phase during 1960-1990 and a negative tendency after 1990 (Fig. S8h), the net effect of the external forcings on the NPGO-like mode in CESM1 LE shows no significant impact (Fig. S8). This might be related to the stronger sensitivity of aerosol-cloud radiation impact in CESM2, which may outweigh the response to GHG emissions (Gettelman et al., 2019). This is evident from the stronger SST response observed over the Pacific in CESM2 aerosol-only simulations (Fig. 1d) compared to the SST mean state response of CESM1 aerosol forcing (Fig. S9). Although models may exhibit different responses to anthropogenic forcing, removing the ensemble mean trends in models also eliminates their differences in mean state changes. As a result, the mean-removed method shows no changes in ensemble mean of PDO and NPGO in CESM1 (Fig. S10) consistent with the results in CESM2 (Fig. 3).

Most of the CMIP6 large ensembles capture the PDO-like pattern as the first mode (Fig. S11a) and the NPGO-like pattern as the second mode (Fig. S12a). Results from CMIP6 large ensembles again indicate that the long-term response in PDV could be associated with the forced mean state change. Ensemble mean time series for both the PDO and NPGO show an externally forced response, with a positive trend before the 1980s and a negative trend afterward (Fig. S11b), consistent with results from CESM2 (Fig. 1e). External forcing also strengthens the pattern of the PDO-like mode, as seen from the 'projection' method in CMIP6 (Fig. S11c). When the ensemble mean is removed from each model, the forced responses disappear from both modes (Figs. S11f & S12f).

However, there is a noticeable increase in ensemble spread in each model with greater intermodal differences when using the 'projection' method (Fig. S11d) compared to the traditional method (Fig. S11b). Larger uncertainty among the models may imply that the projection method is more sensitive to differences between models. Externally forced patterns differ among climate models, leading to major differences in the 'projection' method (Fig. S11d): the PDO time series responds to forcing in the ensemble mean of some models, while it does not for others.

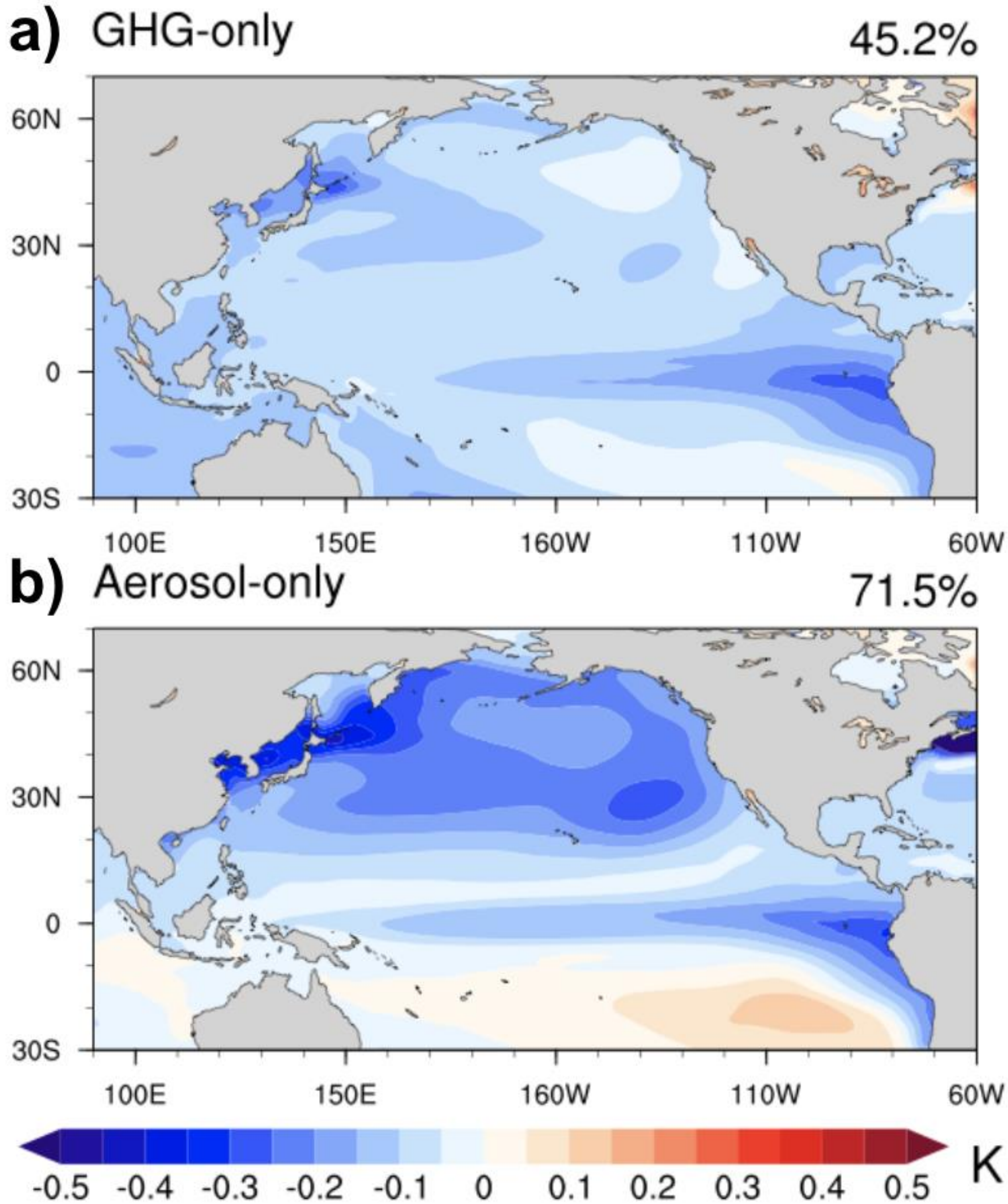

Figure S1. Spatial patterns of SST mean state changes in CESM2 GHG and aerosol single-forcing simulations (1920-2014), represented by the first EOF mode of the SST ensemble mean after GMSST removed (units: K; see Section 2.3).

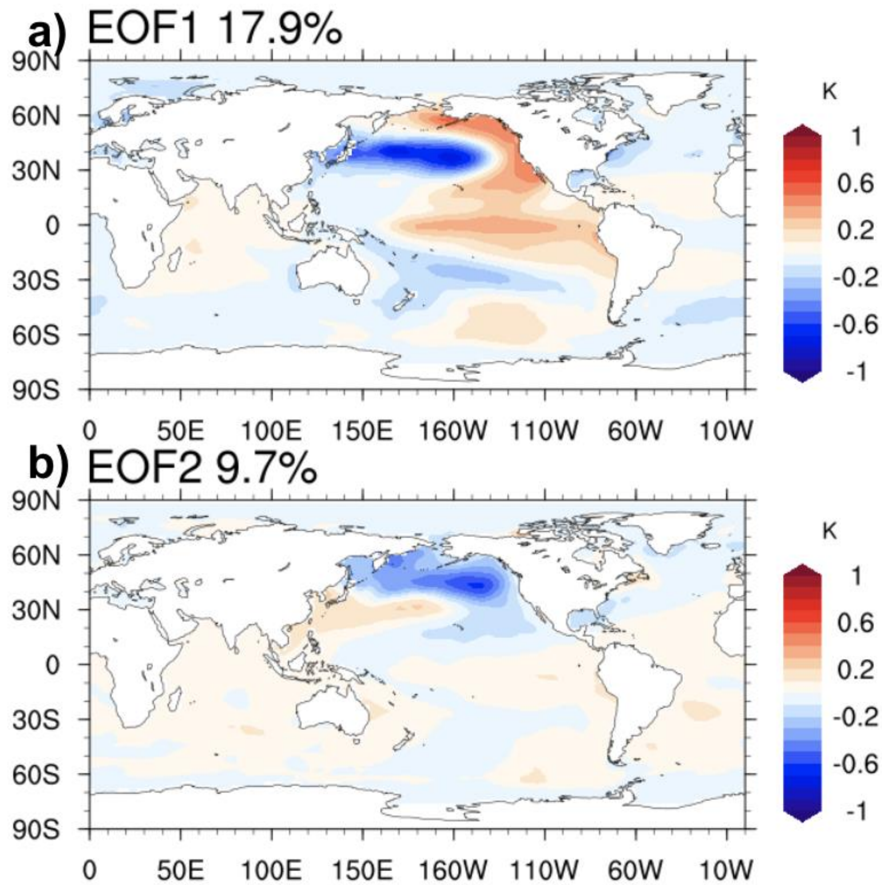

Figure S2. Two leading modes, the PDO mode and the NPGO mode, in observations over 1920-2014. Regression of SSTA onto the first and second EOF over the North Pacific after removing global mean SST in NOAA Extended Reconstructed SST V5 (ERSSTv5;

https://psl.noaa.gov/data/gridded/data.noaa.ersst.v5.html). The percentage of explained variance is displayed at the top of each panel.

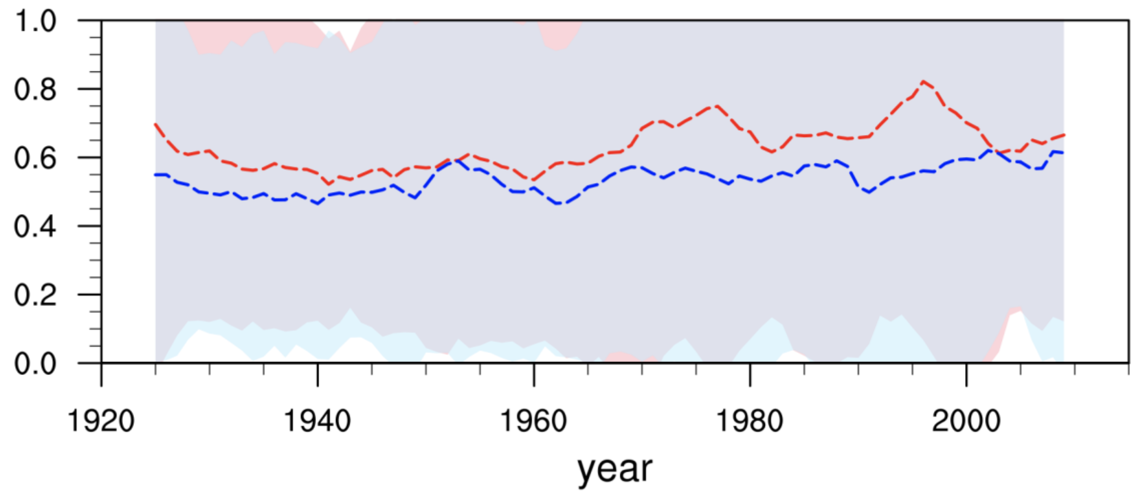

Figure S3. 10-year moving variance of PCs from the traditional method in CESM2 full-forcing. The red (PC1) and blue (PC2) dashed lines show 10-year moving variance of PDV.

i

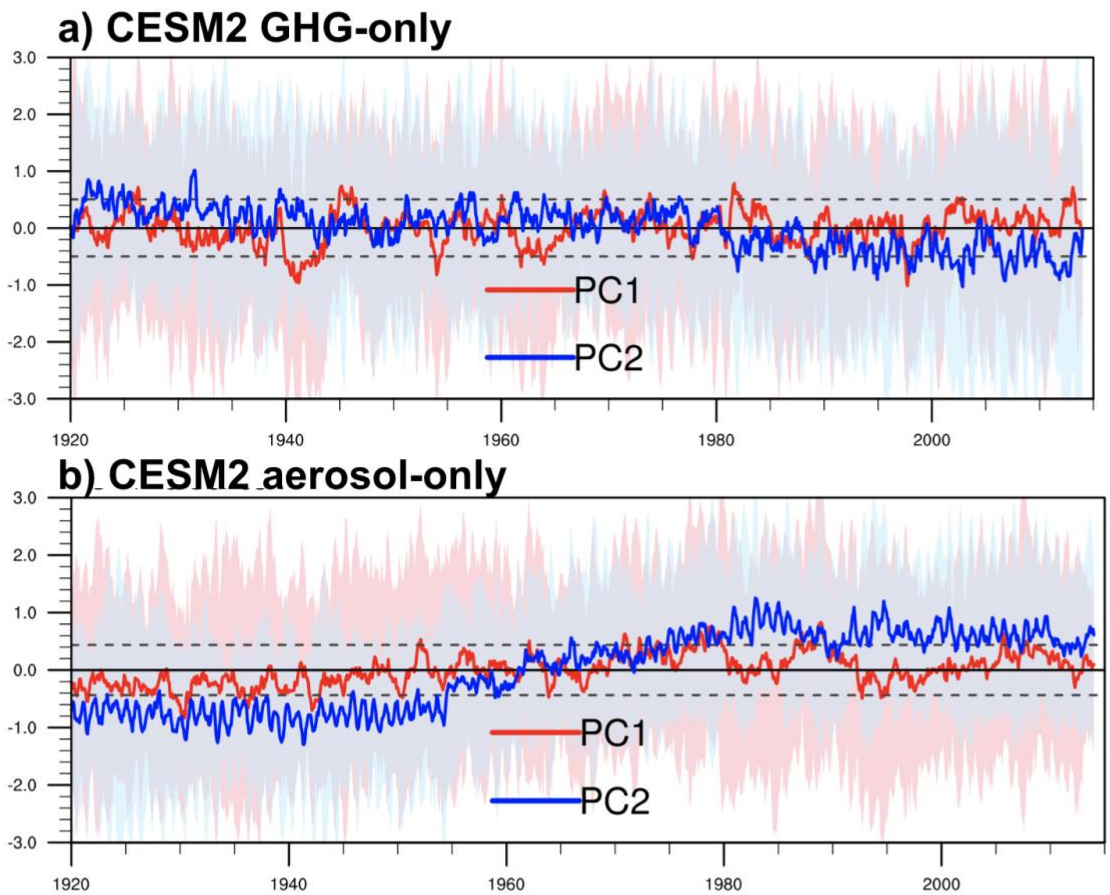

Figure S4. Time series of the first two leading modes of PDV through the traditional method in a) CESM2 GHG-only and b) CESM2 aerosol-only simulations. Similar to Fig. 1e but for single forcing simulations. The red (blue) dash line indicates 10-year moving variance of the PC1 (PC2). Shading in e) represents one standard deviation among ensemble members, while the solid thick lines represent the ensemble mean. The 2.5%

and 97.5% confidence bounds, obtained through 10,000 bootstrap samples, are shown as black dashed lines.

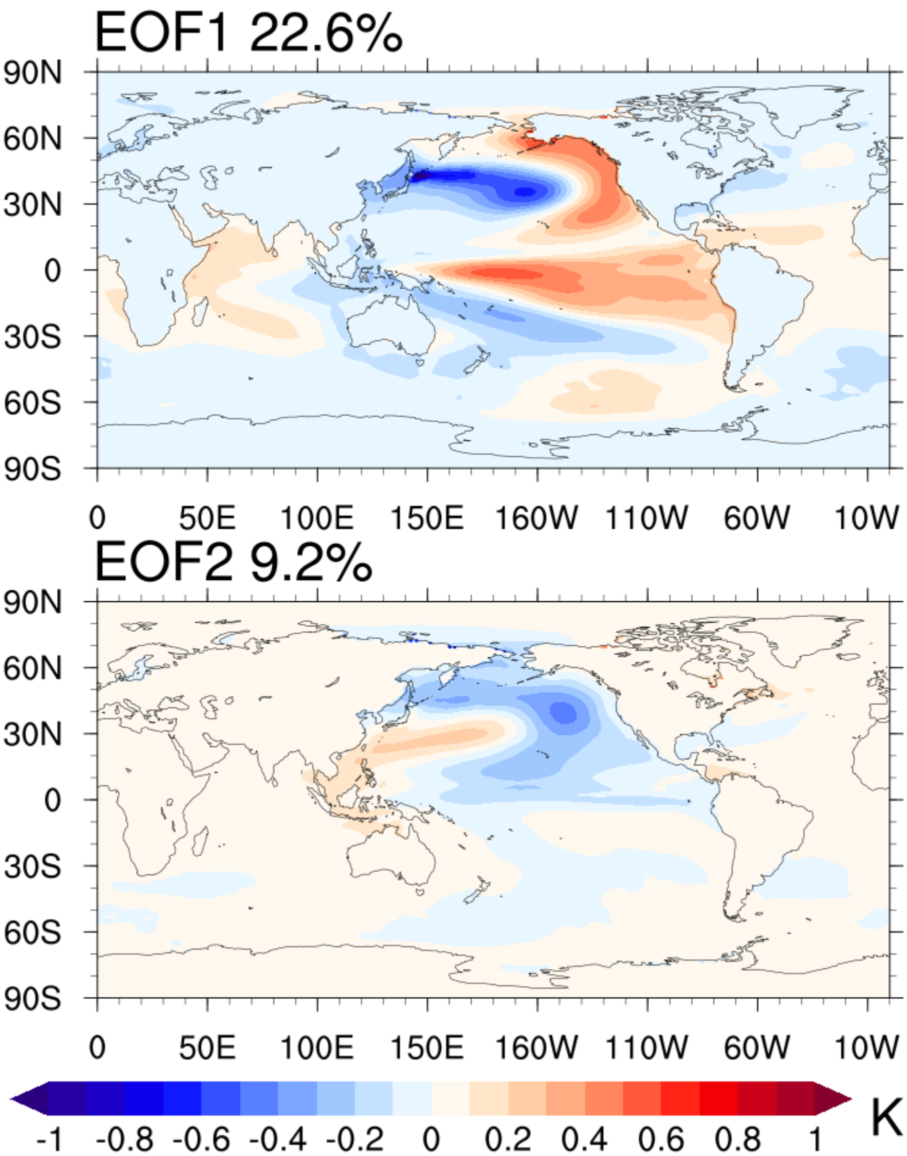

Figure S5. The two major modes in CESM2 preindustrial control runs. EOF on monthly anomalous SST outputs over the North Pacific Ocean with global mean SST removed. The percentage of explained variance is displayed at the top of each panel.

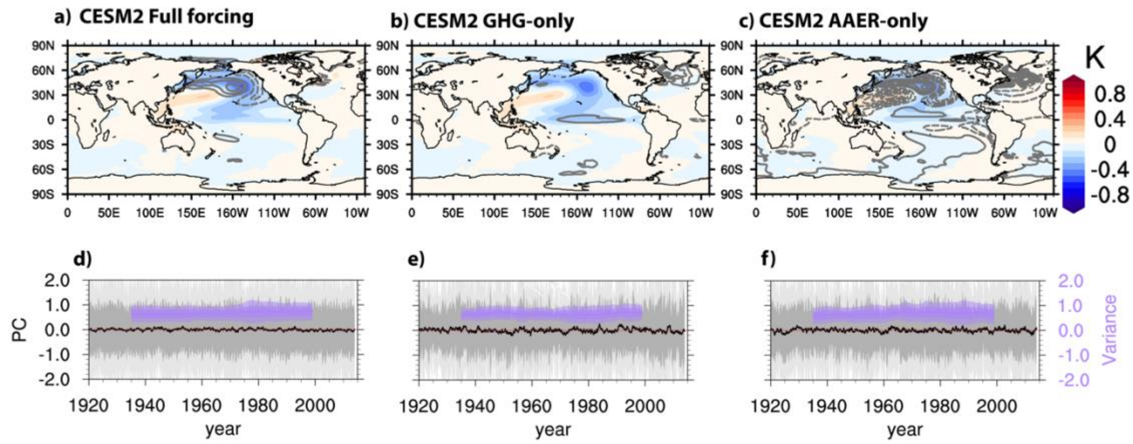

Figure S6. Similar to Figure 3 but for the EOF2 using the mean removed method in CESM2 full-forcing, GHG-only and aerosol-only simulations.

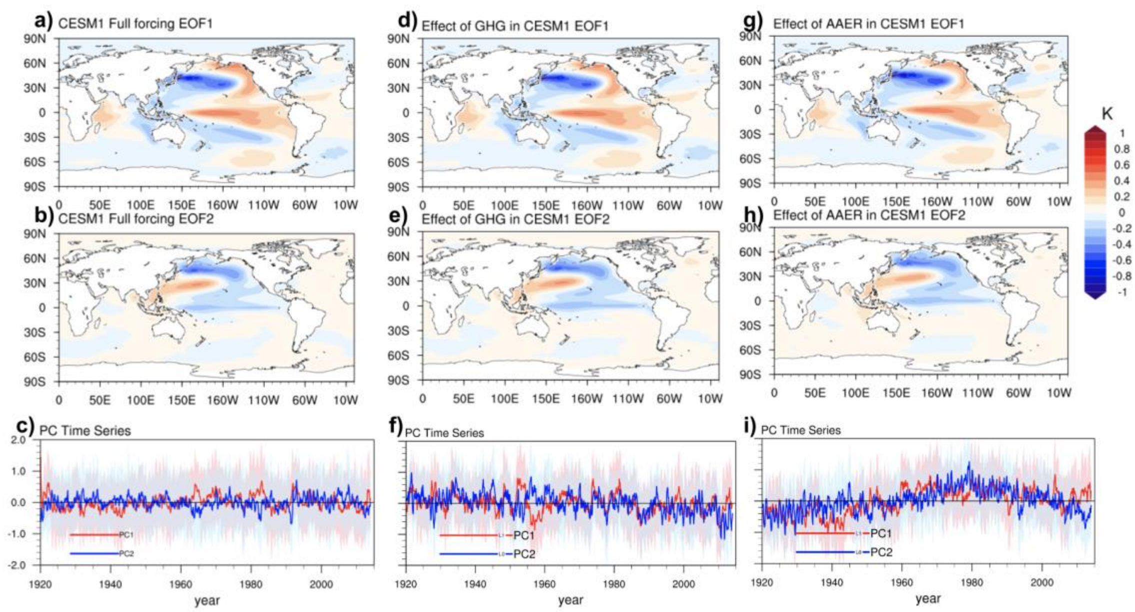

Figure S7. The spatial patterns and time series of the first two major modes using the traditional method in CESM1 a-c) full forcing, d-f) GHG and g-i) aerosols single forcing ensembles. Shading in c), f), i) represents one standard deviation among ensemble members, while the solid thick lines represent the ensemble mean.

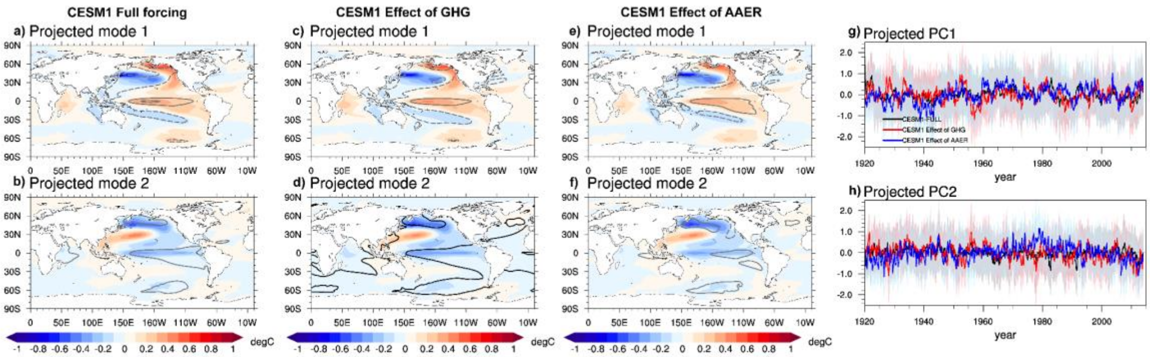

Figure S8. The major Pacific SST modes using the projection method in CESM1. Similar to Figure 2 but for CESM1 full-forcing and all-but-one forcing runs.

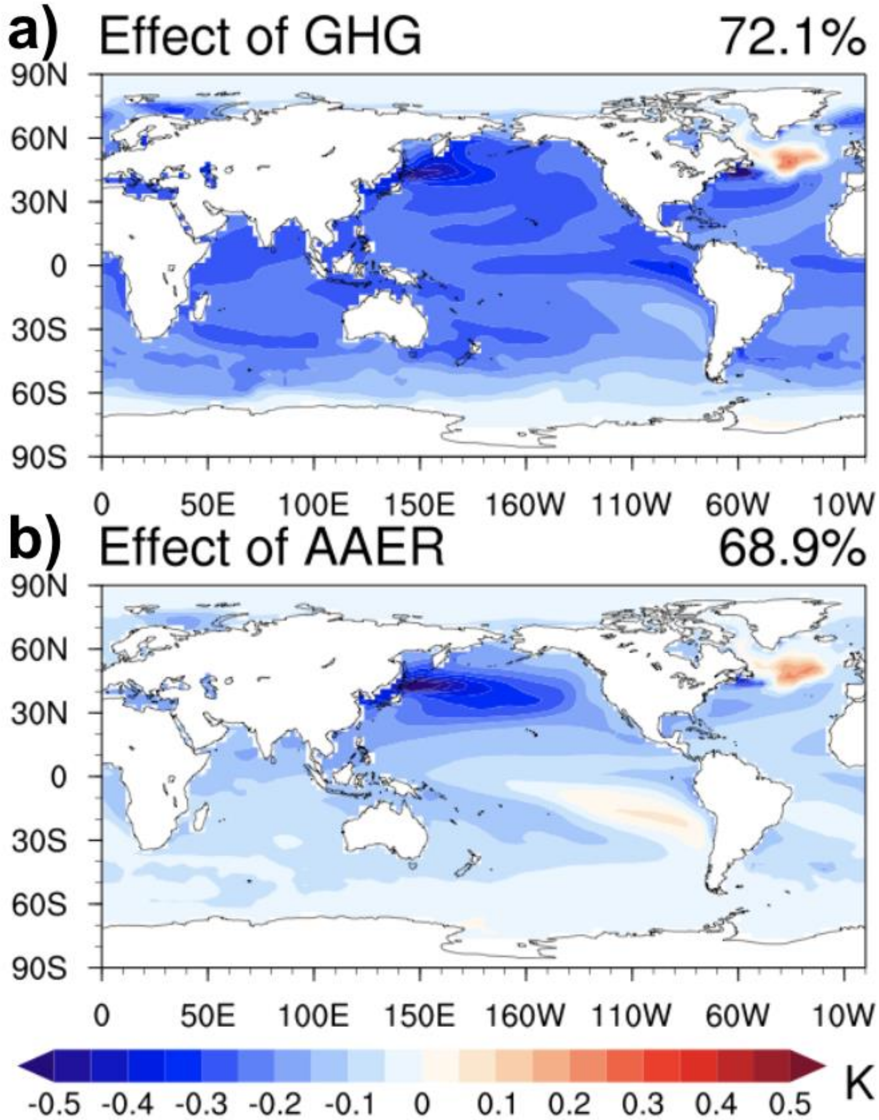

Figure S9. Similar to Fig. S1 but for the CESM1 mean state SST change patterns of a) GHG effect and b) aerosol effect based on CESM1 all-but-one forcing simulations (see Text S1).

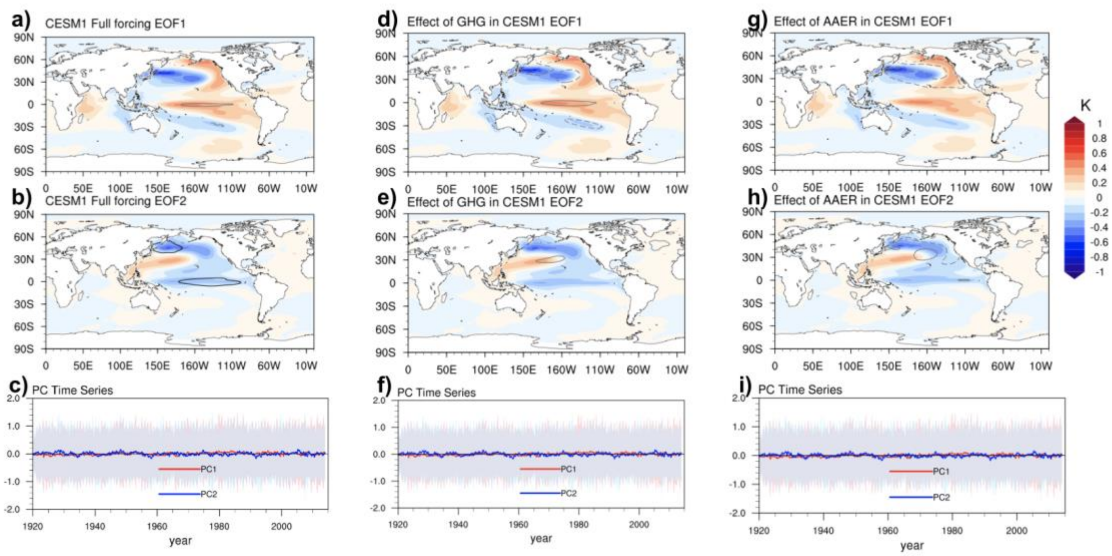

Figure S10. The spatial patterns and time series of the first two major modes using the ensemble mean removed method in CESM1 LE full forcing and all-but-one simulations.

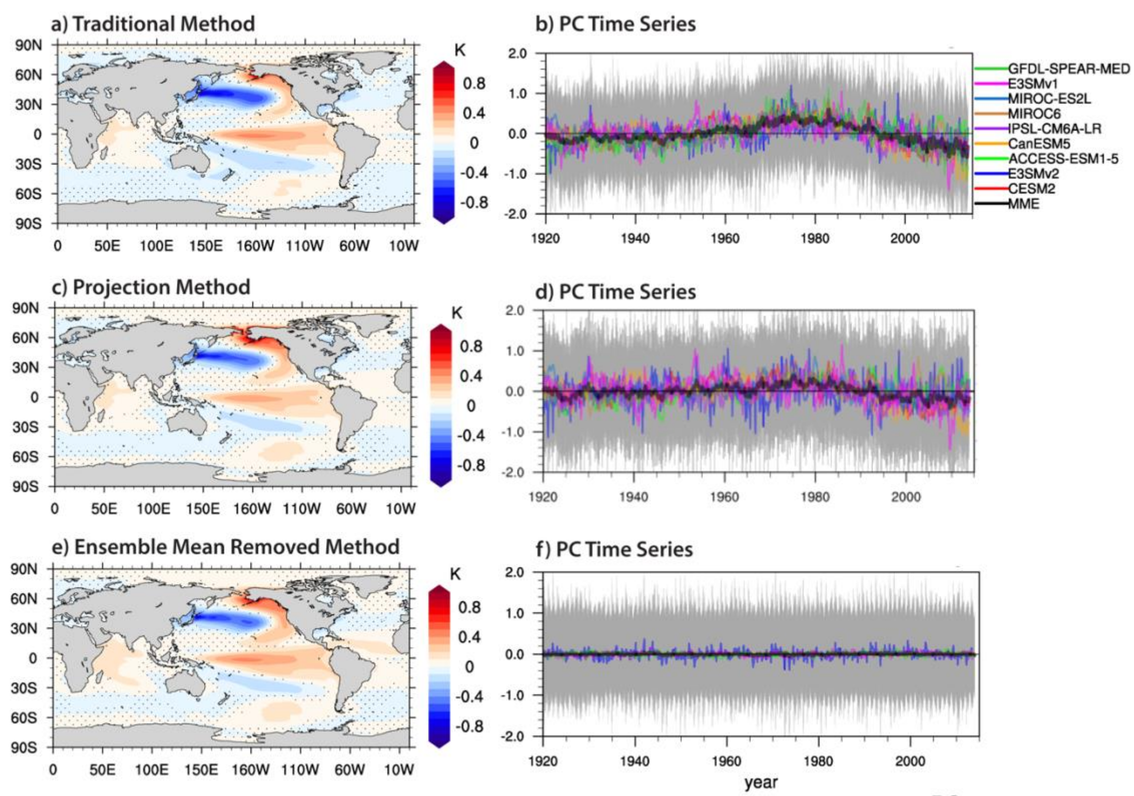

Figure S11. PDO changes using the three analysis methods in CMIP6 full forcing large ensembles (a complete list of CMIP6 models is provided in Table S2). Left column: multi-model mean regression spatial patterns for EOF1 calculated through the a) traditional, c) 'projection' and e) 'mean removed' methods. Stippling in a) indicates that less than 90% of ensemble means agree on the sign of the EOF1 loading through the binomial test. Right column: time series of PC1 of each CMIP6 model through the b) traditional, d) projection and f) ensemble mean removed methods. Shading in b), d) and f) represents one standard deviation of ensemble spread in each model while the solid lines represent the ensemble mean for each ensemble. The time series of multi-model ensemble mean is shown as a black solid line.

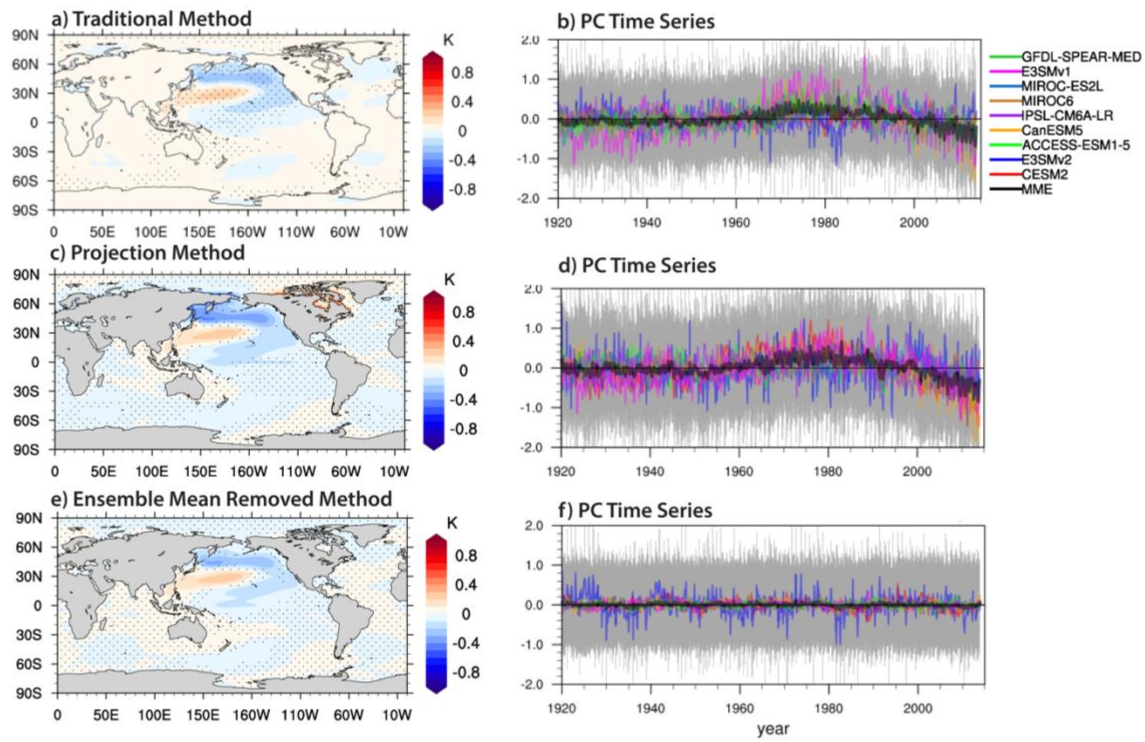

Figure S12. Same as Figure S11 but for the second mode of Pacific SSTA, in CMIP6 full forcing ensembles.

i

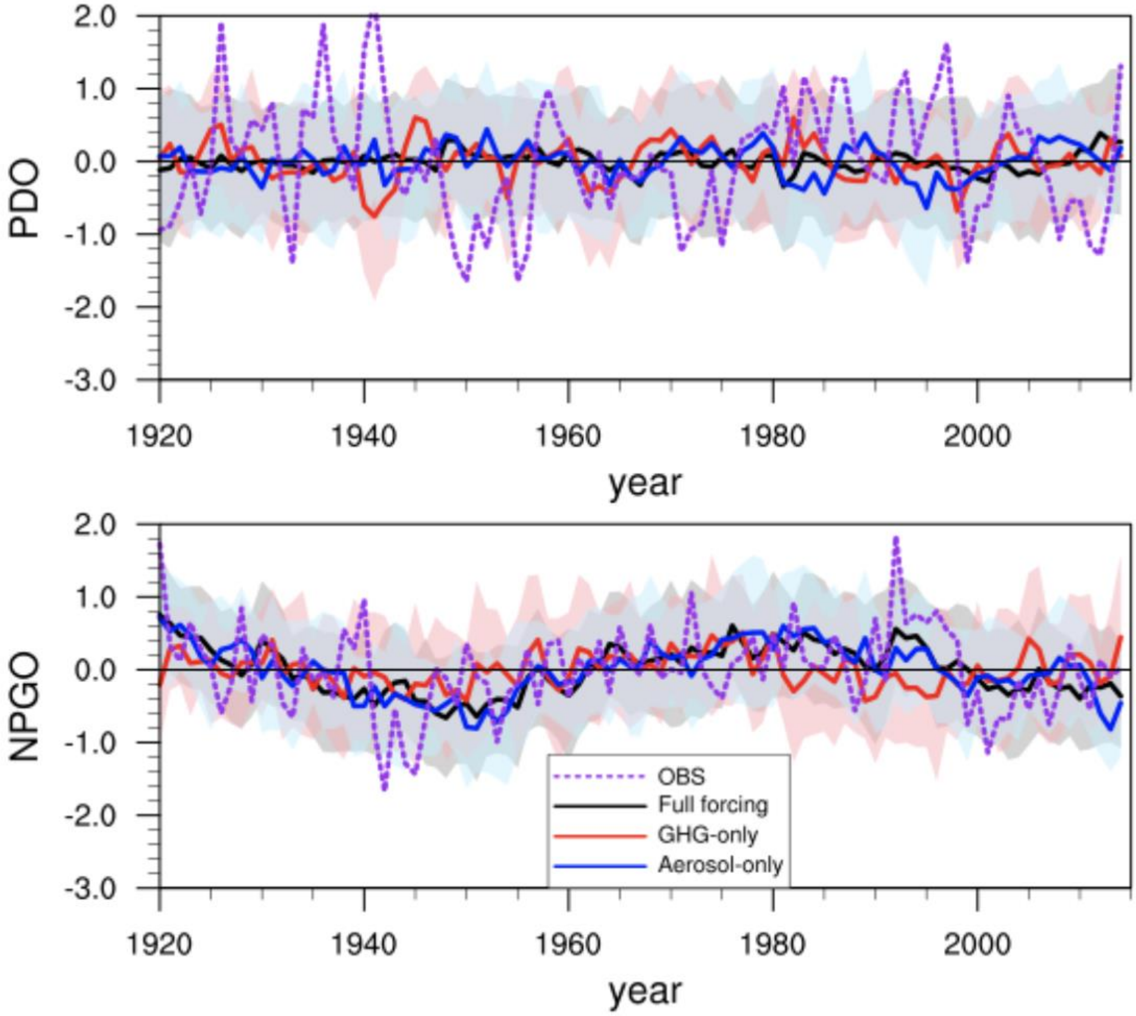

Figure S13. Demonstration of using a quadratic detrend to remove the SST mean state response in observations and CESM2 LE. This corresponds to Figs. 4a & 4b but using the quadratic detrending method rather than removing the GMSST.

Models	Ensemble size	Forcing	Time
CESM1-LE	40	Full	1920-2015
CESM1-XGHG	20	All but GHG	1920-2015
CESM1-XAER	20	All but anthropogenic aerosol	1920-2015
CESM2-LE	50	Full forcing with smoothed BMB (called CESM2-smbb)	1850-2015
CESM2-GHG	15	GHG Only	1850-2015
CESM2-AAER	20	Anthropogenic Aerosol Only	1850-2015

Table S1. Information on CESM simulations used in this study. All CESM1 experiments use the CMIP5 version of the specified forcing, while CESM2 simulations use the CMIP6 updates for each forcing time series.

Modeling Center	Models	Ensemble size	Reference
CSIRO	ACCESS-ESM1-5	40	Ziehn et al. 2020
DOE	E3SMv1	18	Stevenson et al. 2023
DOE	E3SMv2	20	Fasullo et al. 2024
CCCma	CanESM5	40	Swart et al. 2019
GFDL	GFDL-SPEAR-MED	30	Delworth et al. 2020
IPSL	IPSL-CM6A-LR	30	Boucher et al. 2020
MIROC	MIROC6	50	Tatebe et al. 2019
MIROC	MIROC-ES2L	30	Hajima et al. 2020

Table S2. CMIP6 large ensembles used in this study and their ensemble size. Surface temperature over the ocean is used for E3SMv2 to represent sea surface temperature since their ocean variables are missing. We cannot find the preindustrial run for GFDL-SPEAR-MED, so GFDL-SPEAR-MED is not corporated in the projection method. Data compiled and regridded by Maher et al, 2023; & Brunner et al 2020.

Model	Traditional method	Mean removed method
CESM2 Full forcing	22.8% (11.8%)	20.3% (10.9%)
CESM2 GHG-only	21.3% (12.1%)	21.7% (12.2%)
CESM2 Aerosol-only	21.1% (14.4%)	22.0% (10.1%)
CESM1 Full forcing	24.8% (14.1%)	25.3% (15.0%)
CESM1 GHG effect	25.1% (15.0%)	24.0% (17.4%)
CESM1 Aerosol effect	26.0% (15.1%)	27.8% (16.5%)
ACCESS-ESM1-5	17.9% (10.9%)	16.9% (10.7%)
E3SMv1	17.8% (11.7%)	17.6% (11.0%)
E3SMv2	14.9% (11.7%)	15.0% (11.7%)
CanESM5	19.3% (8.9%)	17.0% (8.3%)
GFDL-SPEAR-MED	16.9% (11.6%)	15.1% (10.6%)
IPSL-CM6A-LR	15.8% (10.6%)	14.2% (9.6%)
MIROC6	27.9% (11.6%)	25.3% (11.6%)
MIROC-ES2L	27.9% (10.8%)	25.1% (11.0%)

i

Table S3. Ensemble mean percentage of variance explained in EOF1 (EOF2) using either the traditional method or the mean-removed method in each large ensemble.

References

Boucher, O., Servonnat, J., Albright, A. L., Aumont, O., Balkanski, Y., Bastrikov, V., et al. (2020). Presentation and Evaluation of the IPSL-CM6A-LR Climate Model. Journal of Advances in Modeling Earth Systems, 12(7), e2019MS002010. https://doi.org/10/ghkv9n

Delworth, T. L., Cooke, W. F., Adcroft, A., Bushuk, M., Chen, J.-H., Dunne, K. A., et al. (2020). SPEAR: The Next Generation GFDL Modeling System for Seasonal to Multidecadal Prediction and Projection. Journal of Advances in Modeling Earth Systems, 12(3), e2019MS001895. https://doi.org/10.1029/2019MS001895

Fasullo, J. T., Golaz, J.-C., Caron, J. M., Rosenbloom, N., Meehl, G. A., Strand, W., et al. (2024). An overview of the E3SM version 2 large ensemble and comparison to other E3SM and CESM large ensembles. Earth System Dynamics, 15(2), 367–386. https://doi.org/10.5194/esd-15-367-2024

Gettelman, A., Hannay, C., Bacmeister, J. T., Neale, R. B., Pendergrass, A. G., Danabasoglu, G., et al. (2019). High Climate Sensitivity in the Community Earth System Model Version 2 (CESM2). Geophysical Research Letters, 46(14), 8329–8337. https://doi.org/10.1029/2019GL083978

Hajima, T., Watanabe, M., Yamamoto, A., Tatebe, H., Noguchi, M. A., Abe, M., et al. (2020). Development of the MIROC-ES2L Earth system model and the evaluation of biogeochemical processes and feedbacks. Geoscientific Model Development, 13(5), 2197–2244. https://doi.org/10.5194/gmd-13-2197-2020

Stevenson, S., Huang, X., Zhao, Y., Di Lorenzo, E., Newman, M., van Roekel, L., et al. (2023). Ensemble Spread Behavior in Coupled Climate Models: Insights From the Energy Exascale Earth System Model Version 1 Large Ensemble. Journal of Advances in Modeling Earth Systems, 15(7), e2023MS003653. https://doi.org/10.1029/2023MS003653

Swart, N. C., Cole, J. N. S., Kharin, V. V., Lazare, M., Scinocca, J. F., Gillett, N. P., et al. (2019). The Canadian Earth System Model version 5 (CanESM5.0.3). Geoscientific Model Development, 12(11), 4823–4873. https://doi.org/10.5194/gmd-12-4823-2019

Tatebe, H., Ogura, T., Nitta, T., Komuro, Y., Ogochi, K., Takemura, T., et al. (2019). Description and basic evaluation of simulated mean state, internal variability, and climate sensitivity in MIROC6. Geoscientific Model Development, 12(7), 2727–2765. https://doi.org/10/ghkv9q

Touma, D., Stevenson, S., Lehner, F., & Coats, S. (2021). Human-driven greenhouse gas and aerosol emissions cause distinct regional impacts on extreme fire weather. Nature Communications, 12(1), 212. https://doi.org/10.1038/s41467-020-20570-w

Ziehn, T., Chamberlain, M. A., Law, R. M., Lenton, A., Bodman, R. W., Dix, M., et al. (2020). The Australian Earth System Model: ACCESS-ESM1.5. Journal of Southern Hemisphere Earth Systems Science, 70(1), 193–214. https://doi.org/10.1071/ES19035

i